POLITECNICO
MILANO 1863

Spacecraft Attitude Dynamics and Control

Final Project

Mario Corradetti
952839

Academic Year 2021-2022

Nomenclature

μ	Gravitational parameter
Ω	Right ascension of the ascending node
ω	Argument of perigee or Angular velocity
θ	True anomaly
a	Semi-major axis
$A_{b/n}$	Attitude matrix
c	Speed of light
e	Eccentricity
F_e	EM power per unit surface
h	Angular momentum
i	Inclination
M_c	Control torque
M_d	Disturbance torque
ADCS	Attitude Determination Control System
CG	Center of Gravity
CMG	Control Moment Gyroscope
DCM	Direction Cosine Matrix
GG	Gravity Gradient
I	Inertia matrix or Identity matrix
LVLH	Local Vertical Local Horizontal
SRP	Solar Radiation Pressure

Contents

1 Introduction

The purpose of the following report is to investigate the Attitude Determination and Control of a 3U CubeSat in an orbit from the Orbital Mechanics project.The design of the Attitude Determination Control System is tested and proven through the propagation of the dynamics for one orbit. The simulation, performed with Matlab and Simulink, will account for the presence of disturbance torques along with the actual performances of the selected Attitude Determination Control System components, while neglecting the effect of perturbations upon the orbit because of the different timescales considered.

1.1 Satellite configuration

The satellite under consideration is a 3U CubeSat, Fig. 1, for terrestrial ground observation. It requires ground pointing of the payload instruments (in satellite's $-x$-axis, with 1° of accuracy) and the three axis stabilization in order to track the LVLH frame. It is equipped with a 3U Deployable Solar Array (in satellite y-axis). Spacecraft's dimension and mass are reported in Table 1:

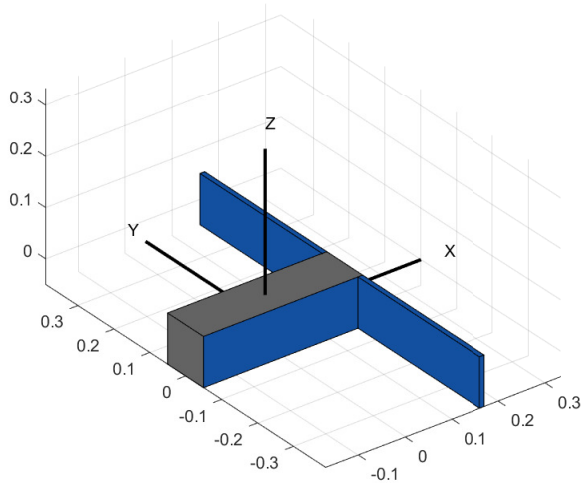

Figure 1: 3U CubeSat model

	Mass[kg]	Dimension [mm]
Structure+Payload	3.5	100x100x340.5
Solar Array	0.270	100x681x1.6

Table 1: CubeSat specifics

It is assumed that the origin is coincident with the center of mass, reducing the matrix to a diagonal form confirming that the principal axes are used. Furthermore, the inertia matrix respects the inequalities constraints for the inertia moments.

$$\boldsymbol{I} = \begin{bmatrix} 0.0118 & 0 & 0 \\ 0 & 0.0469 & 0 \\ 0 & 0 & 0.0456 \end{bmatrix} \text{ kg}\cdot\text{m}^2$$

$$\underline{r}_{CG} = \begin{bmatrix} 0.0105 & 0 & 0 \end{bmatrix} \text{ m}$$

1.2 Orbit parameters

The orbit selected, Fig. 2, is the one from the Orbital Mechanics project, the orbit parameters are shown in Table 2:

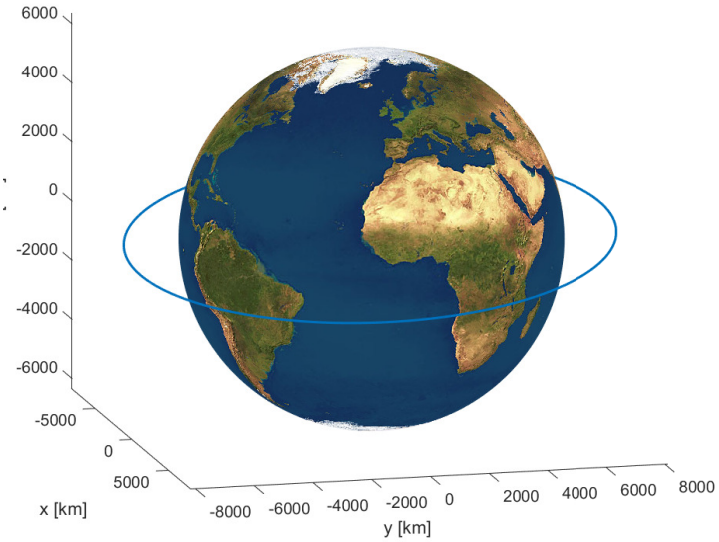

Figure 2: Orbit representation

a $[km]$	e	i[°]	Ω[°]	ω[°]
8150	0.0054	7.9875	64.26	348.04

Table 2: Orbit parameter

1.3 Sensors

The spacecraft has been equipped with the following sensors:

1.3.1 Magnetometer - *NanoSense M315 GomSpace*

Compact tri-axial low noise fluxgate magnetometers[7], Fig. 3, whose datasheet is shown in Table 3:

Figure 3: NanoSense M315

Range$[\mu T]$	rate$[Hz]$	Dimension$[mm]$	Mass$[g]$	Noise$[nT]$
$\pm$800	10	23x20x8	8	15

Table 3: M315 specifications

1.3.2 Earth Horizon Sensor - *CubeSense N*

Compact Nadir sensor with integrated electronics[2], Fig. 4, whose datasheet is shown in Table 4:

Figure 4: CubeSense N

FOV[°]	Rate$[Hz]$	Dimension $[mm]$	Mass$[g]$	Accuracy[°]
$\sim$ 180	2	41.7x17.7x24.3	30	$<$0.2

Table 4: CubeSense N specifications

1.3.3 Sun Sensor - *FSS100 Nano Fine*

2 axis digital Sun sensor[5], Fig. 5 , embedded with calibration error table whose datasheet is shown in Table 5 :

Figure 5: FSS100

FOV[°]	Rate[Hz]	Dimension [mm]	Mass[g]	Accuracy[°]
120	8	20x10x5.7	<0.5	0.1

Table 5: CubeSense N specifications

1.3.4 Gyroscope - *STIM210*

Multi-axis gyro module[8], Fig. 6, whose datasheet is shown in Table 6:

Figure 6: STIM210

Rate[Hz]	Dimension [mm]	Mass[g]	ARW [$°/\sqrt{h}$]	RRW [$°/h$]
250	45x39x22	52	0.15	0.3

Table 6: STIM210 specifications

1.4 Actuators

1.4.1 Reaction wheel - BCT Micro Reaction Wheel

Highly capable CubeSat reaction wheel[1], Fig. 7, whose datasheet is shown in Table 7:

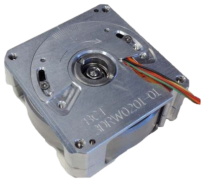

Figure 7: BCT

Dimension [mm]	Mass[g]	Torque [mNm]	Momentum [$mNms$]
43x43x18	150	0.6	18

Table 7: BCT specifications

1.4.2 Inertia wheel

As preliminary design an inertia wheel with the same specifications of the reaction wheel has been chosen.

2 Model

2.1 Attitude Dynamics and Kinematics

In the analysis of the the spacecraft dynamics, it is common practice to de-couple orbital mechanics and attitude dynamics, due their very different time scales. As a result we may neglect the translational component between the inertial frame and the body frame. The mathematical model adopted is based on the Euler's equation of motion :

$$\mathbf{I}\dot{\underline{\omega}} = \mathbf{I}\underline{\omega} \wedge \underline{\omega} + \underline{M_d} + \underline{M_c} \tag{1}$$

Where $\underline{\omega}$ is the angular velocity of the satellite, $\underline{M_c}$ represents the control torque, that will be analyzed section 5, and $\underline{M_d}$ represents the external disturbance torques, all of them expressed in the body reference frame.

It has been chosen to compute the CubeSat attitude kinematics by means of its Direction Cosine Matrix $\mathbf{A}(t)$; once $\underline{\omega}$ has been evaluated/measured the differential equation that rules the kinematic is evaluated using the following relation :

$$\frac{d\mathbf{A}_{B/N}}{dt} = -[\underline{\omega}\wedge]\mathbf{A}_{B/N}(t) \tag{2}$$

$\mathbf{A}$ is the rotation matrix from the inertial to the body frame and $[\cdot\wedge]$ is the cross product matrix operator. In order to preserve the orthogonality property of the rotation matrix $\mathbf{A}$ at each time step the following algorithm has been applied :

$$\mathbf{A}_k = \frac{3}{2}\mathbf{A}_{k-1} - \frac{1}{2}\mathbf{A}_{k-1}\mathbf{A}_{k-1}^T\mathbf{A}_{k-1} \tag{3}$$

2.2 Disturbing Torques

The main disturbances perturbing the spacecraft attitude are the following:

- Magnetic torque
- Solar Radiation Pressure (SRP)
- Gravity gradient
- Atmospheric drag

For this analysis all of them have been taken into account except for the atmospheric drag, that can be totally neglected due the height of the orbit.

2.2.1 Magnetic torque

For a precise modeling of the Earth's magnetic field, the latter might be expressed in an Earth-rotating frame as the gradient of a potential function given by a series expansion of spherical harmonics. For our purpose a simplified dipole-model has been considered to be sufficient. The magnetic field vector in inertial frame, $\underline{b}_N$, is computed as :

$$\underline{b}_N = \frac{R_{Earth}^3 H_0}{r^3}\left[3(\underline{\hat{m}}\cdot\underline{\hat{r}}_N)\underline{\hat{r}}_N - \underline{\hat{m}}\right] \tag{4}$$

where $\underline{\hat{r}}_N$ is the versor in the direction of the spacecraft in inertial reference frame, while $\underline{\hat{m}}$ is the unit dipole vector. The latter can be computed as follows:

$$\underline{\hat{m}} = \begin{bmatrix} sin(11.5°)cos(\omega_{Earth}t) \\ sin(11.5°)sin(\omega_{Earth}t) \\ cos(11.5°) \end{bmatrix} \tag{5}$$

The term H_0 is computed from the first order Gaussian coefficient of the IRGF such that:

$$H_0 = \sqrt{\left(g_1^0\right)^2 + \left(g_1^1\right)^2 + \left(h_1^1\right)^2} \tag{6}$$

The Gaussian coefficients g_n^m, h_n^m are subjected to time variation over the years and their experimental values are known up to 13^{th} order. The magnetic disturbance torque is caused by the interaction between Earth's magnetic field and the residual magnetic induction due on-board currents. Such parasitic induction is difficult to model, it has been assumed to be $\underline{m} = [0.01 \;\; 0.05 \;\; 0.01]^T Am^2$.The corresponding disturbance torque has been computed as :

$$\underline{M}_{d,magnetic} = \underline{m} \wedge \underline{b_B} \tag{7}$$

where $\underline{b}_B = \mathbf{A}_{B/N}\underline{b}_N$.

2.2.2 Solar Radiation Pressure

The SRP is caused by the impact of the photons on the surfaces of the photon on the surfaces of the spacecraft. The major source of this disturbance is the Sun, however also Earth gives its contribution, because of the reflection of the Sun radiation and its own radiation. We can split the electromagnetic radiation level by three contributions:

- Direct solar radiation : $1367\frac{W}{m^2}$
- Solar radiation reflected by Earth (Albedo) : $400\frac{W}{m^2}$
- Earth's own radiation : $103\frac{W}{m^2}$

In order to evaluate the disturbance torque, the satellite's external surface is divided into several planar surfaces (defined by normal unit vector $\underline{n}$) and the overall torque is computed as the superposition of each contribution. Each surface is associated with a given specular and diffuse reflection coefficients, respectively ρ_s and ρ_d. It is assumed that $\rho_{s,i} = 0.1$ for the solar panels, $\rho_{s,i} = 0.5$ for the surface of the main body, and $\rho_{d,i} = 0.1$ for all the surfaces. The Sun position in the inertial reference frame is known from an on-board model, which, assuming that the Sun direction with respect to the spacecraft can be approximated as the Sun direction with respect to the Earth, is based on:

$$\underline{\hat{s}}_B = \mathbf{A}_{B/N}\underline{\hat{s}}_N = \mathbf{A}_{B/N}\begin{Bmatrix} cos(n_{Sun}t) \\ sin(n_{Sun}t)cos(23.45°) \\ sin(n_{Sun}t)sin(23.45°) \end{Bmatrix} \tag{8}$$

t is the time, $\epsilon = 23.45°$ is the tilting of the Earth axis with respect to the ecliptic plane and n_{Sun} is the velocity of the apparent motion of the Sun around the Earth. Then, it is rotated by means of the DCM in order to obtain the Sun direction in the body frame ($\underline{\hat{s}}^B$). It is possible to compute the disturbance torque as :

$$\underline{M}_{d,SRP} = \sum_i (\underline{r}_i \wedge \underline{F}_i) \tag{9}$$

$\underline{F}_i$ is the force acting on the i-th surface and can be computed as:

$$\underline{F}_i = \begin{cases} -PA_i(\hat{S_B} \cdot \hat{N_{Bi}}) \left[(1-\rho_s)\hat{S}_B + (2\rho_s(\hat{S}_B \cdot \hat{N}_{Bi}) + \frac{2}{3}\rho_d)\hat{N}_{Bi}\right] & \hat{S}_B \cdot \hat{N}_{Bi} > 0 \\ 0 & \hat{S}_B \cdot \hat{N}_{Bi} < 0 \end{cases} \tag{10}$$

where $P = \frac{F_e}{c}$, with F_e, EM power per unit surface, and c, speed of light.

2.2.3 Gravity Gradient

The gravity gradient torque is naturally embedded in the satellite configuration since it depends on its inertia properties, its orientation with respect to the Earth and its distance from the center of the Earth. The torque can be computed as :

$$\underline{M}_{d,GG} = \frac{3\mu}{||\underline{r}_{sc}||^3}\begin{Bmatrix} (I_z - I_y)c_2c_3 \\ (I_x - I_z)c_1c_3 \\ (I_y - I_x)c_2c_1 \end{Bmatrix} \tag{11}$$

where :

$$\begin{Bmatrix} c_1 \\ c_2 \\ c_3 \end{Bmatrix} = \mathbf{A}_{B/N}\mathbf{A}^T_{LVLH/N}\begin{Bmatrix} 1 \\ 0 \\ 0 \end{Bmatrix} = \mathbf{A}_{B/LVLH}\begin{Bmatrix} 1 \\ 0 \\ 0 \end{Bmatrix}$$

$\mathbf{A}^T_{B/LVLH}$ is the rotation matrix from the inertial to the Local Vertical Local Horizontal frame.

2.3 Sensors

2.3.1 Earth Horizon Sensor, Sun Sensor and Magnetometer

The model includes sensor, not in terms of their physical behaviour but in terms of the quality of measurement they provide. With this assumption, the position of the Earth and Sun perceived by the respective sensors is described as the perturbation of the real one through a alignment error variable with time :

$$r^B_{measured} = \mathbf{A}_{B/Sensor}\mathbf{A}_\epsilon(t) r^{Sensor}_{measured} \tag{12}$$

The values of the off-diagonal terms are generated with independent normal distributions with zero mean and variance associated to the accuracy of the sensor. In the case of the magnetometer:

$$r^B_{measured} = \mathbf{A}_{B/Sensor}\left(\mathbf{A}_\epsilon(t)\mathbf{A}_{con} r^{Sensor}_{measured} + \underline{b}\right) r^{Sensor}_{measured} \tag{13}$$

In this case the error matrix $\mathbf{A}_{con}$ is a not orthogonal construction matrix where each axis is assembled one at time[4].

$$\mathbf{A}_{con} = \begin{Bmatrix} 1 & \alpha_{zx} & -\alpha_{yx} \\ -\alpha_{zy} & 1 & \alpha_{xy} \\ \alpha_{yz} & -\alpha_{xz} & 1 \end{Bmatrix} \tag{14}$$

The term $\underline{b}$ is an additive error due to the intrinsic noise of the sensor. In order to minimise also the disturbance from the main body of the spacecraft it is placed as far as possible from the center of the body.

2.3.2 Gyroscope

The implementation of a gyroscope as a sensor is not useful only for the detumbling phase but also when the Earth Horizon and the Sun sensor measures are not available. The measurement of the gyroscope is affected by a noise term and a bias term on the angular velocity output, it is modeled as :

$$\underline{\omega}^B_{measured} = \mathbf{A}_{B/Sensor}\left(\mathbf{A}^T_{B/Sensor}\underline{\omega}^B + \underline{n} + \underline{b}\right) \tag{15}$$

where $\underline{n}$ and $\underline{b}$ are random number and can be represented in the form as :

- Angular Random Walk (ARW) : $\underline{n} = \sigma_n \underline{\xi}_n$ attributed to thermo-mechanical noise of the system, modelled as white Gaussian noise with zero mean and variance depending on the sampling frequency
- Rate Random Walk (RRW) : $\dot{\underline{b}} = \sigma_n \underline{\xi}_b$ attributed to electronic noise of the system, modelled as white Gaussian noise with zero mean and variance depending on the sampling frequency.

2.4 Actuators

2.4.1 Reaction Wheel

The active control actuators are 3 reaction wheels with their axes aligned with the body axes, in order to have a full control of the spacecraft. They can only exchange angular momentum but not produce a net torque. The derivative of the angular momentum of the reaction wheels can be computed as :

$$\dot{\underline{h}}_r = -\mathbf{A}^{-1}_{RW}(\underline{M}_c + \underline{\omega} \wedge \mathbf{A}_{RW}\underline{h}_r) \tag{16}$$

where $\mathbf{A}_{RW}$ expresses the configuration in which the actuators are placed:

$$\mathbf{A}_{RW} = \begin{bmatrix} 1 & 0 & 0 \\ 0 & 1 & 0 \\ 0 & 0 & 1 \end{bmatrix} \tag{17}$$

$\underline{M}_c$ is the control torque computed by the control algorithm. The torque produced by the actuators is :

$$\underline{M}_{RW} = -\left(\mathbf{A}_{RW}\dot{\underline{h}}_r + \underline{\omega} \wedge \mathbf{A}_{RW}\underline{h}_r\right) \tag{18}$$

2.5 Inertia wheel

The inertia wheel is used primarily to provide the spacecraft with the momentum bias necessary for inertial attitude stability. The effect of an inertia wheel can be easily added into the Euler's equation :

$$\mathbf{I}\dot{\underline{\omega}}_B + \underline{\omega}_B \wedge (\underline{h}_B + \underline{h}_{wheel}) = \underline{M}_d + \underline{M}_c \tag{19}$$

where $\underline{h}_{wheel} = \mathbf{I}_{wheel}\underline{\omega}_{wheel}$, the angular velocity of the wheel, $\underline{\omega}_{wheel}$, is the relative one between the wheel and spacecraft. The matrix $\mathbf{I}$ has to take into account also the wheel and not only the spacecraft.

3 Attitude Determination

The attitude determination has the role to estimates the relative position of the spacecraft with respect to another reference frame. In order to do this, the estimation can be done by the knowledge of the angular velocities, computed by the gyroscope, or using measures provided by the sensors. When magnetometer, Sun sensor and Earth horizon work at the same time, the SVD method developed within the framework of Wahba's problem is used. Wahba's problem consists in minimizing the weighted error function :

$$J = \frac{1}{2}\sum_{i=1}^{N} \alpha_i ||\underline{s}_{Bi} - \mathbf{A}_{B/N}\underline{v}_{Ni}||^2 \tag{20}$$

where N sensor measurements, $\underline{s}_i$, are available along with the corresponding esitmation $\mathbf{A}_{B/N}\underline{v}_{Ni}$, while α_i are the weights identifying the sensor precision. The solution of the problem passes through the computation of a matrix $\mathbf{B}$ expressed as :

$$\mathbf{B} = \sum_{i=1}^{N} \alpha_i \underline{s}_i \underline{v}_i^T \tag{21}$$

The DCM representing the attitude of the spacecraft is retrieved as :

$$\mathbf{A} = \mathbf{U}\mathbf{M}\mathbf{V}^T \tag{22}$$

in which :

- $\mathbf{U}$ is composed by the eigenvectors of $\mathbf{B}\mathbf{B}^T$
- $\mathbf{V}$ is composed by the eigenvector of $\mathbf{B}^T\mathbf{B}$
- $\mathbf{M} = diag(\ 1 \quad 1 \quad det(\mathbf{U}) \quad det(\mathbf{V})\ )$

Once implemented this procedure an observer is introduced in order to filter out the noise derived from the sensor measurements. Its dynamics is based on the same equation that govern the kinematics in terms of DCM, at which we add the observer term :

$$\frac{d\mathbf{A}_{est}}{dt} = -[\omega\wedge]\mathbf{A}_{est} + G(\mathbf{A}_{raw} - \mathbf{A}_{est}) \tag{23}$$

where $\mathbf{A}_{raw}$ is the one obtained through the SVD.
When the Sun is out of the Sun sensor's FOV an algebraic method is used. This method requires 2 measures, $\underline{p}$ and $\underline{q}$, and their relative value computed by an on-board model, $\underline{a}$ and $\underline{b}$. The method make use of the following procedure :

$$\begin{aligned} \underline{s}_1 &= \underline{p} & \qquad \underline{v}_1 &= \underline{a} \\ \underline{s}_2 &= \frac{\underline{p}\wedge\underline{q}}{|\underline{p}\wedge\underline{q}|} & \qquad \underline{v}_2 &= \frac{\underline{a}\wedge\underline{b}}{|\underline{a}\wedge\underline{b}|} \\ \underline{s}_3 &= \underline{p}\wedge\underline{s}_2 & \qquad \underline{v}_3 &= \underline{a}\wedge\underline{v}_2 \end{aligned}$$

$$\begin{aligned} \mathbf{S} &= [\ \underline{s}_1 \quad \underline{s}_2 \quad \underline{s}_3\ ] \\ \mathbf{V} &= [\ \underline{v}_1 \quad \underline{v}_2 \quad \underline{v}_3\ ] \\ \mathbf{A}_{B/N} &= \mathbf{S}\mathbf{V}^{-1} = \mathbf{S}\mathbf{V}^{T} \end{aligned} \tag{24}$$

During the detumbling phase could happen that both the Sun and the Earth are out the field of view of the respective sensors. Since is not possible to determine the attitude with only one measure the measured angular velocity is used to propagate the attitude through the integration of Eq. (2).

4 Mission Overview

Objective of the mission is to achieve a constant alignment between the $x-$axis of the body frame ($\hat{\underline{x}}_B$) and the $x-$axis of the LVLH frame ($\hat{\underline{x}}_L$). Performance parameter of the mission is the pointing error, which is the angle between the two axis and can be computed as :

$$\text{Pointing error} = \arccos(\hat{\underline{x}}_B^T\hat{\underline{x}}_L) = \arccos\left(\begin{bmatrix} 1 & 1 & 1 \end{bmatrix}\mathbf{A}_{B/N}\mathbf{A}_{L/N}^T\begin{bmatrix} 1 \\ 0 \\ 0 \end{bmatrix}\right) \tag{25}$$

The mission is composed by three control modes:

- **Detumbling** : decrease the angular velocity of the spacecraft after the separation of the launcher.
- **Slew maneuver** : the spacecraft has to be re-oriented in order to reach the desired alignment between the body frame and the LVLH frame.
- **Earth pointing** : the pointing error must be reduced and maintained below 1°.

5 Control Algorithms

The entire implementation of control is entrusted to the 3 reaction wheels. In fact, these are able to provide an efficient detumbling and 3-axis stabilization.

5.1 Detumbling

The detumbling of the spacecraft is implemented during the span of 400s. The ideal control law used is a simple P-controller function of the angular velocity:

$$\underline{M}_c = -k_p\underline{\omega}^B_{measured} \tag{26}$$

A proportional tuning parameter, chosen by a trial and error method, of $k_p = 0.001$ is used.

5.2 Slew maneuver - Earth pointing

Objective of the controller is keeping the spacecraft principal axes aligned with the LVLH frame in order to maintain the payload and the Earth Horizon sensor in front of the Earth. The error matrix, on which the controller will act is given at each time step by :

$$\mathbf{A}_{err} = \mathbf{A}_{B/N}\mathbf{A}_{LVLH/N}^{T} \tag{27}$$

where $\mathbf{A}_{B/N}$ is obtained by integrating Eq. (23).
$\mathbf{A}_{err}$ must be, as more as possible, close to the identity matrix. Then the proportional part of a PD-controller will operate on its off-diagonal terms with the aim of keeping them close to zero. The derivative part will operate on the difference between the actual angular velocity of the satellite and the angular velocity of the LVLH frame[3], with the aim of making them coincident. The control law[6] can be expressed as:

$$\begin{cases} M_{c,x} = -k_{p,x}\left[\mathbf{A}_{err}(2,3) - \mathbf{A}_{err}(3,2)\right] - k_{d,x}(\omega_x - \omega_{LVLH,x}) \\ M_{c,y} = -k_{p,y}\left[\mathbf{A}_{err}(3,1) - \mathbf{A}_{err}(1,3)\right] - k_{d,y}(\omega_y - \omega_{LVLH,y}) \\ M_{c,z} = -k_{p,z}\left[\mathbf{A}_{err}(1,2) - \mathbf{A}_{err}(2,1)\right] - k_{d,z}(\omega_z - \omega_{LVLH,z}) \end{cases} \tag{28}$$

A proportional tuning parameter of $k_p = 0.0003$ and a derivative tuning parameter of $k_d = 0.01$ are used. As the detumbling phase, also the gains of the PD have been chosen with a trial and error approach.

6 Simulation Framework

A conceptual block scheme of the ADCS is presented in Fig. 8.

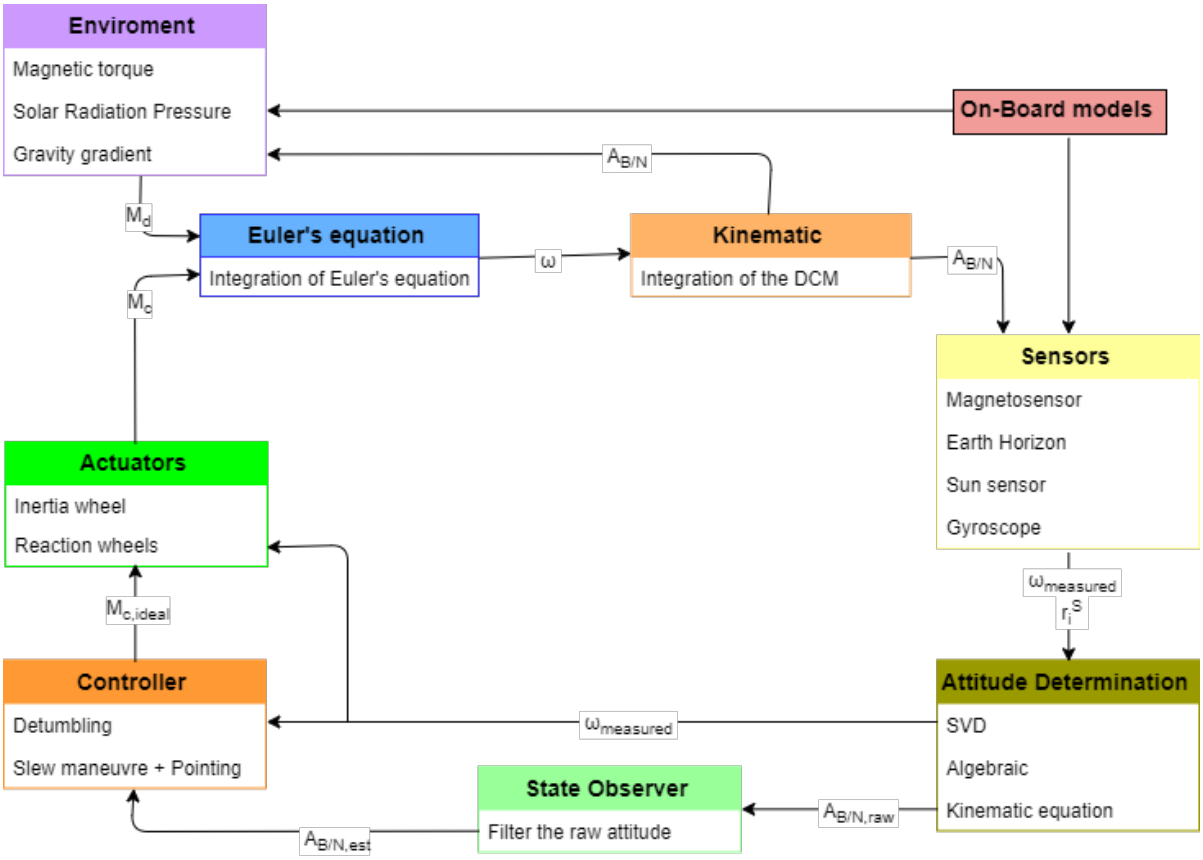

Figure 8: Simulation scheme

7 Simulation Results

The attitude dynamics of the satellite is first analyzed in the uncontrolled case, then in the controlled one. Both cases have been carried out for one full orbital period.

7.1 Uncontrolled case

The simulation has been carried out with the following initial condition :

$$\theta(0) = 0° \quad \omega(0) = [\ 0.1 \quad 0.1 \quad 0.1\ ] \quad \mathbf{A}_{B/N}(0) = I$$

The main quantities are reported in Fig. 9.

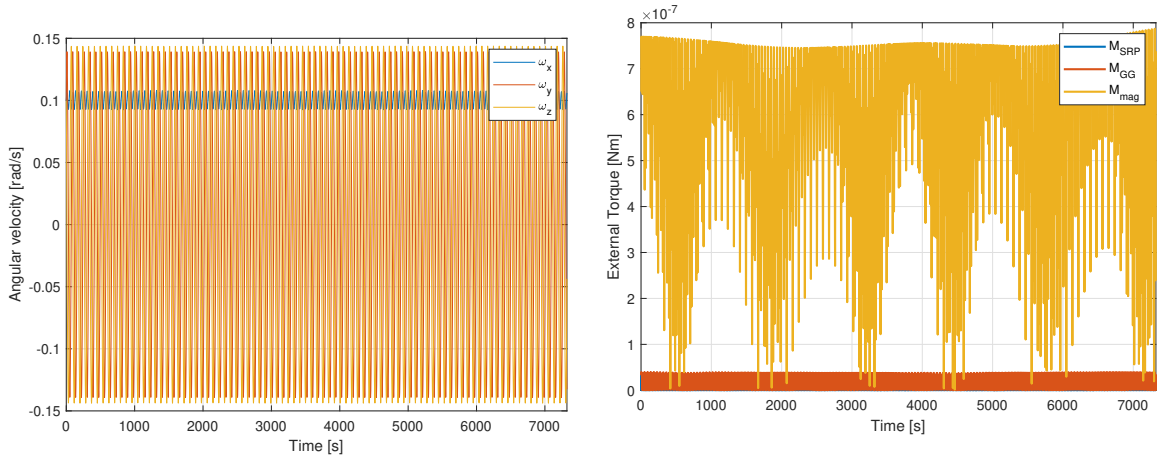

Figure 9: Uncontrolled dynamics

It is easy to notice that the satellite does not oppose in any way to the effects of the disturbing torque and rotate uncontrollably under their actions.

7.2 Controlled case

As for the uncontrolled case, the controlled one has been carried out with the following initial conditions:

$$\theta(0) = 0° \quad \omega(0) = [\ 0.1 \quad 0.1 \quad 0.1\ ]\frac{rad}{s} \quad \mathbf{A}_{B/N}(0) = I$$

The detumbling phase starts at $t = 0$ and lasts for $400s$, after that the controller relative to slew manoeuvre and pointing activates. The results in Fig. 10 show that the control system is capable of reducing angular velocity, as close as possible to the desired one, in the three phases of the mission.

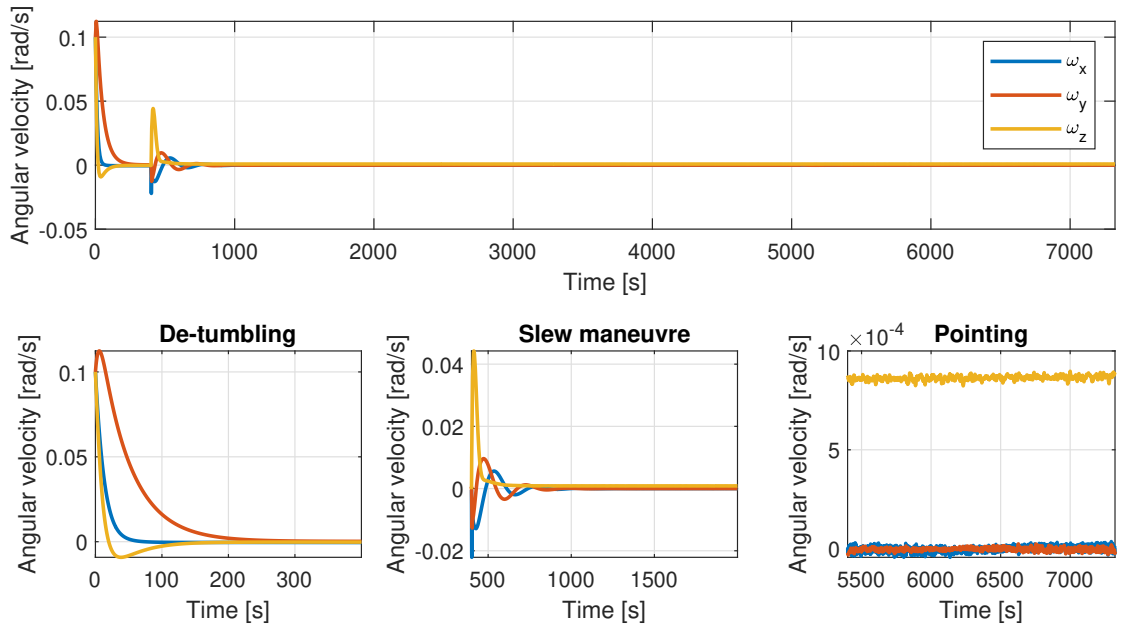

Figure 10: Controlled angular velocity

The behaviour of the pointing error is represented in Fig. 11 :

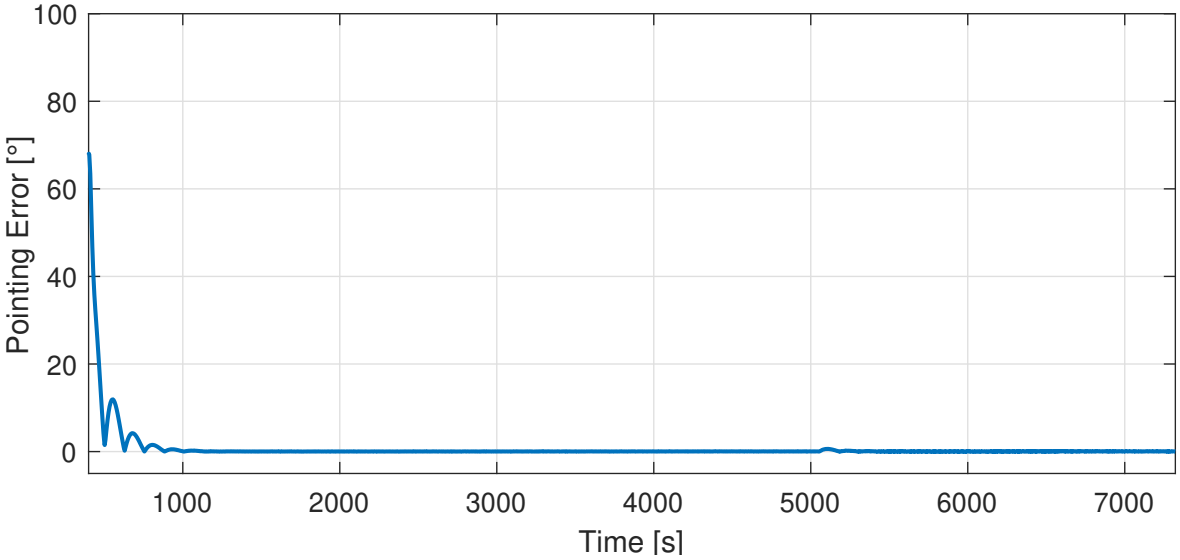

Figure 11: Pointing error

The control acting on the spacecraft is represented in Fig. 12.

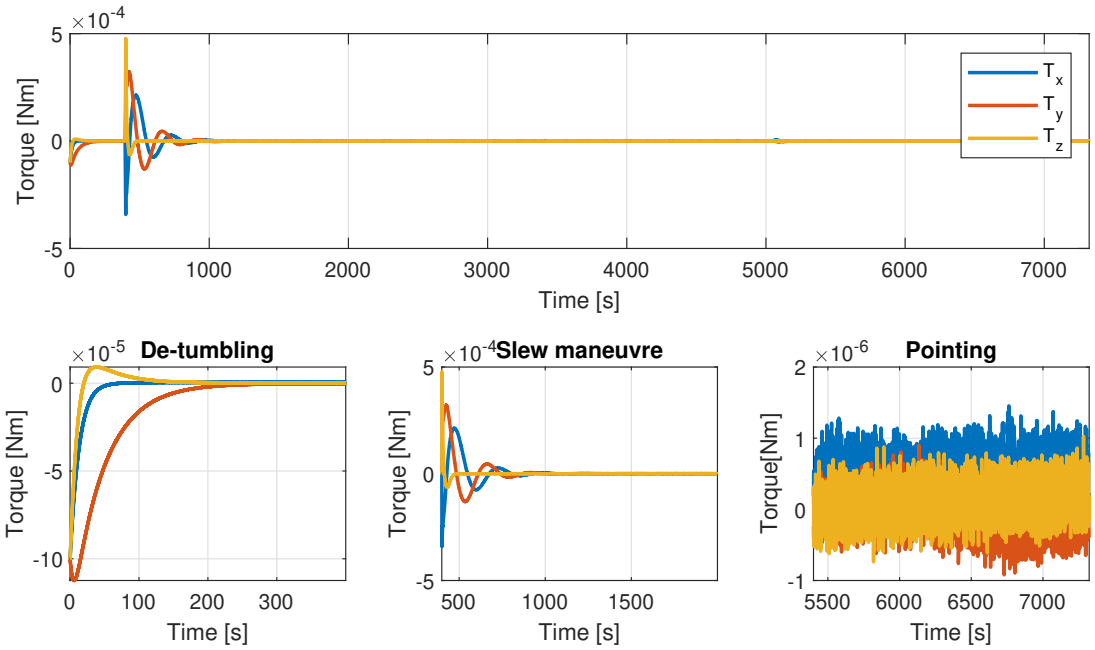

Figure 12: Control torque

The higher control torque during the slew manoeuvre is around the $z-$axis, as expected since it has to bring the $x-$axis from the actual location to the desired one, so a rotation of $\approx 60°$. The control torque affecting the orientation of the spacecraft affects also the magnitude of the external torque, as it can be noticed in Fig. 13 :

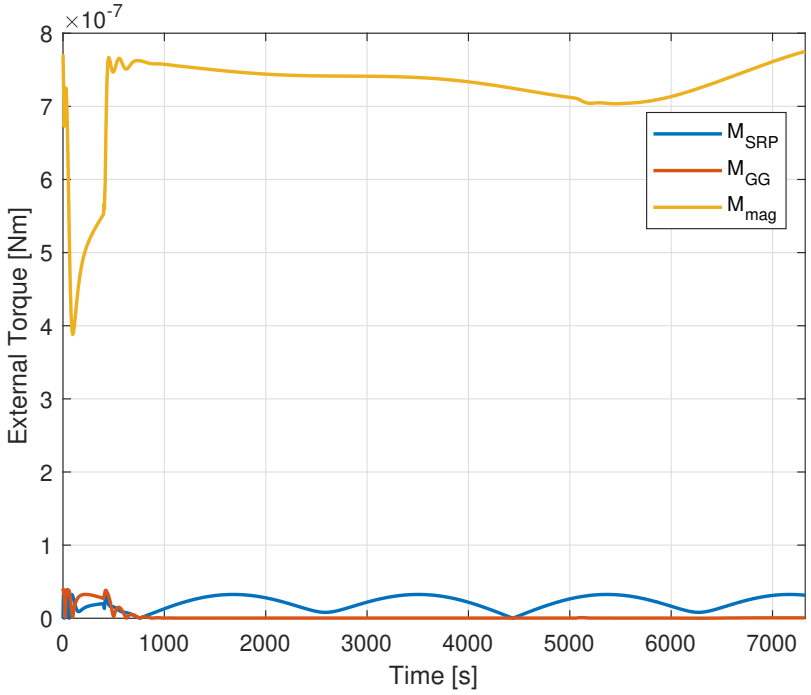

Figure 13: External torque in controlled case

7.3 Off-design case

In order to assure robustness of the ADCS some parameters of the nominal case are changed. Since the main goal of the mission is to align the body frame and the LVLH frame the pointing error is considered as main performance parameter. As first off-design case the gains of the PD-controller, for slew manoeuvre and pointing, have been changed according to the ones in Table 8. The mean values of the pointing error after $t = 2000s$ are shown in Fig. 14:

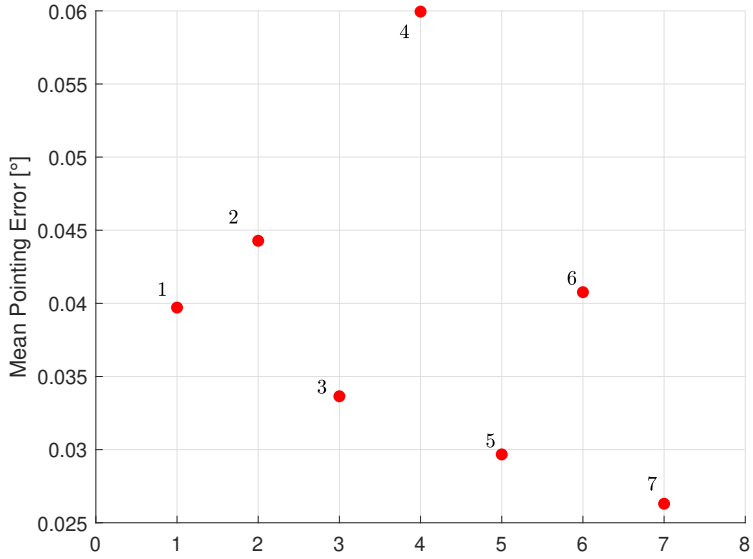

	k_p	k_d
1	3.5×10^{-4}	2×10^{-2}
2	3×10^{-4}	2×10^{-2}
3	4×10^{-4}	2×10^{-2}
4	2.5×10^{-4}	2×10^{-2}
5	3×10^{-4}	2.5×10^{-2}
6	3×10^{-4}	1.5×10^{-2}
7	3×10^{-4}	1×10^{-2}

Table 8: Values of gains

Figure 14: Off-design case 1

In the second off-design case the diameter of the inertia wheel has been changed of $\pm 3mm$, the performance parameter, Fig. 15, is propagated for $t = 2000s$ to appreciate the difference between the different conditions. Moreover the maximum torque required by the reaction wheels have been taken into account in Table 10.

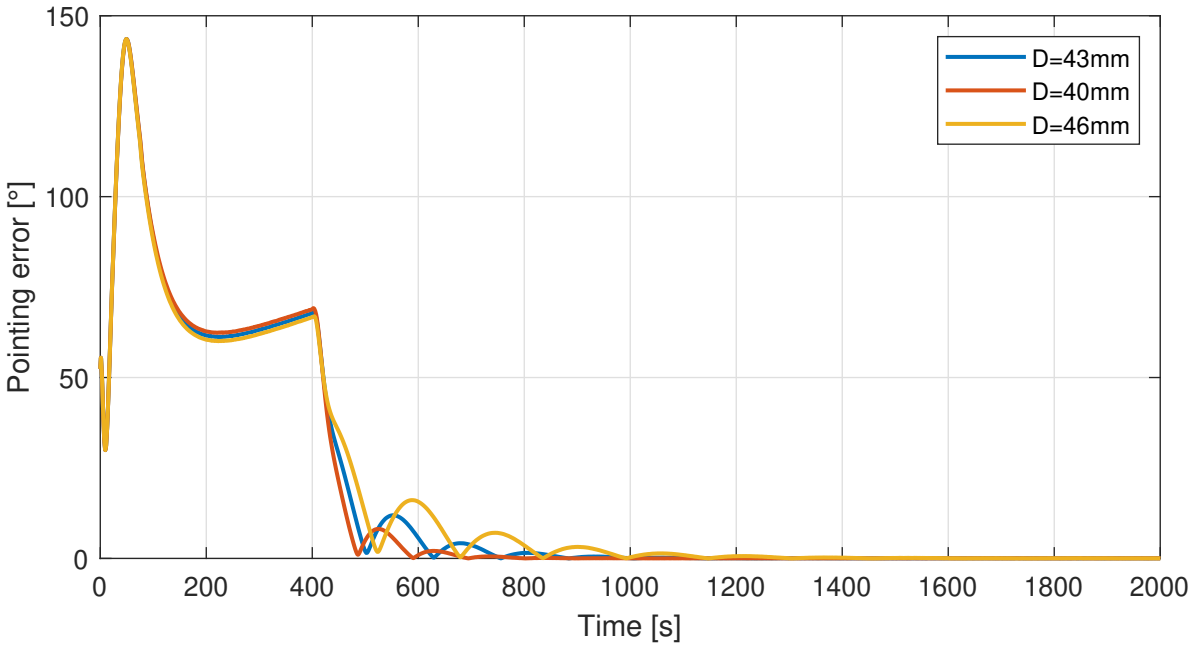

Figure 15: Pointing error off design case 2

	$T_x[Nm]$	$T_y[Nm]$	$T_z[Nm]$
D=43mm	2.1388×10^{-4}	3.2296×10^{-4}	4.7783×10^{-4}
D=40mm	1.7517×10^{-4}	2.9107×10^{-4}	4.8146×10^{-4}
D=46mm	2.5244×10^{-4}	3.5282×10^{-4}	4.7371×10^{-4}

Table 9: Max torque reaction wheel off-design case 2

It can be noticed that an inertia wheel with a smaller diameter would grant higher performance. However, the choice on inertia wheels dimension is limited by the fact that off-the-shelf components are usually employed in CubeSat's mission.

In a third off-design case, an uncertainty of $\pm 0.5kg$ on the spacecraft mass has been assumed. The performance parameter and maximum torque that the reaction wheels have to provide are respectively shown in Fig. 16 and Table 10.

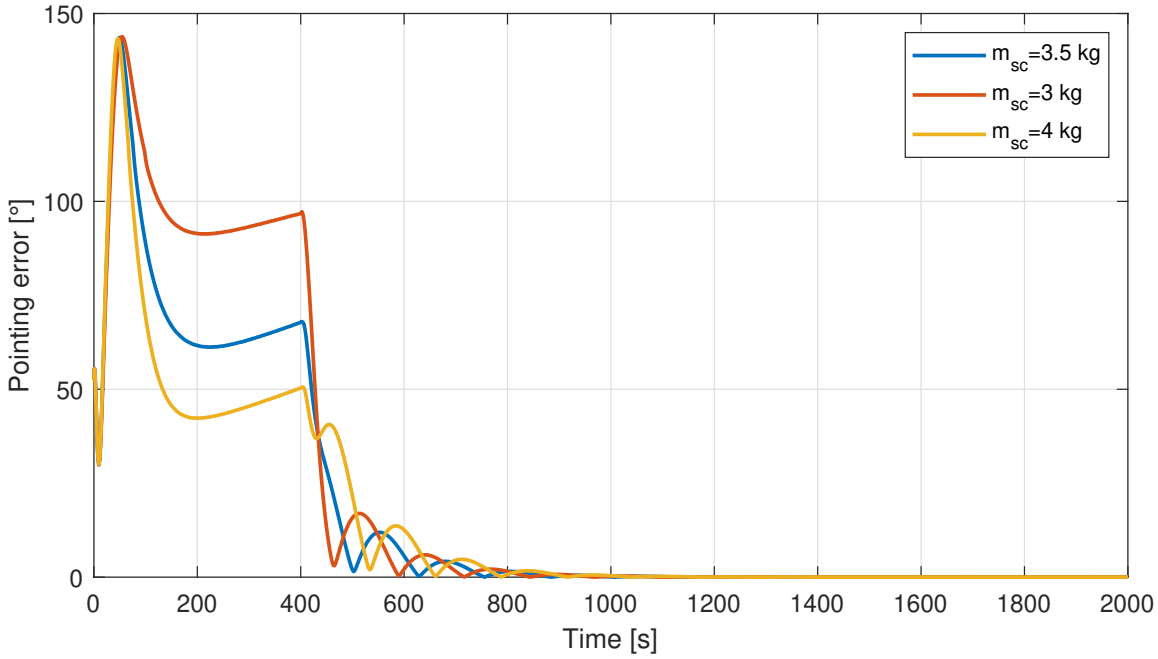

Figure 16: Pointing error off-design case 3

	$T_x[Nm]$	$T_y[Nm]$	$T_z[Nm]$
$m_{sc} = 3.5kg$	2.1388×10^{-4}	3.2296×10^{-4}	4.7783×10^{-4}
$m_{sc} = 3kg$	2.8646×10^{-4}	3.4517×10^{-4}	4.7707×10^{-4}
$m_{sc} = 4kg$	2.4293×10^{-4}	3.8765×10^{-4}	3.6573×10^{-4}

Table 10: Max torque reaction wheel

Intuitively the maximum torque that has to be provided is in correspondence of the beginning of the pointing phase and it is directly proportional to the pointing error in that instant, higher the pointing error higher the torque. A first strategy to reduce the torque in that instant could be to implement a different controller in the detumbling phase that, while reducing the angular velocity as close as possible to zero, tries also to start the alignment of the body frame and LVLH frame.

As last off-design condition a different value for the initial angular velocity has been considered. Considering :

$$\omega(0) = \begin{bmatrix} 0.2 & 0.2 & 0.2 \end{bmatrix}$$

the angular velocity, Fig. 17, control torque, Fig. 18, and pointing error, Fig. 19, can be evaluated.

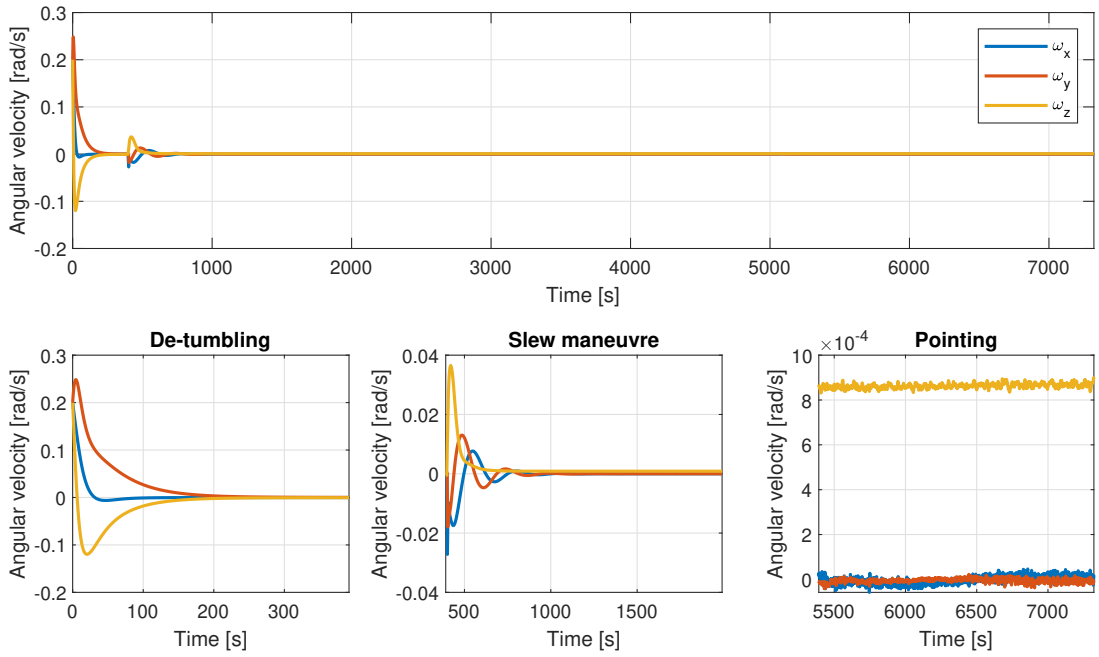

Figure 17: Angular velocities off-design case 4.1

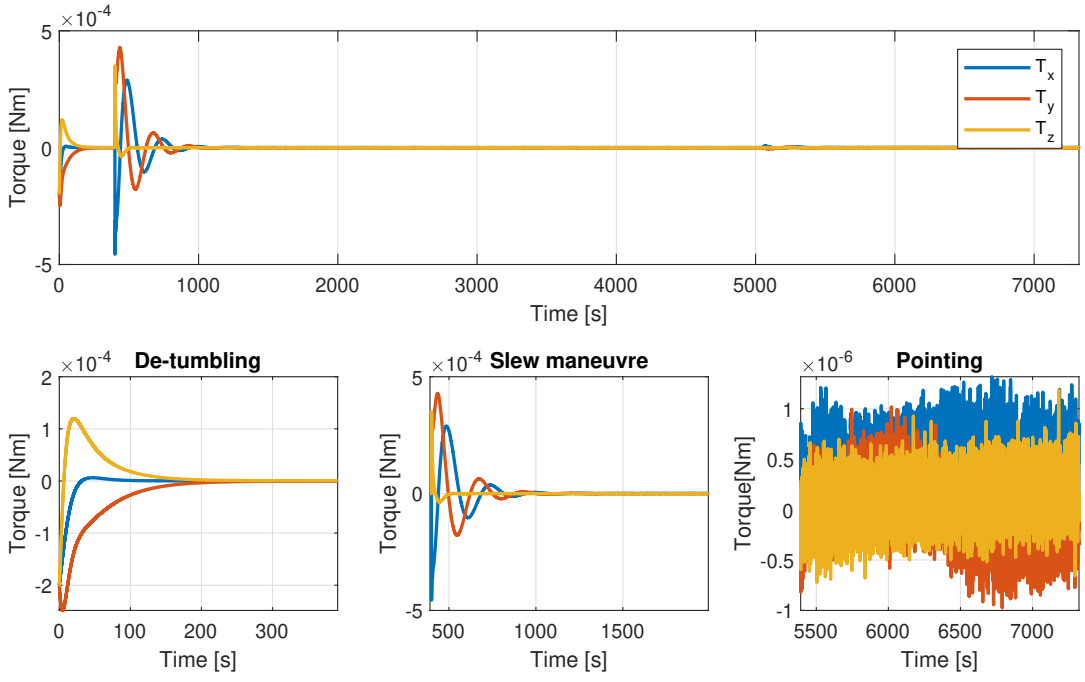

Figure 18: Control torque off-design case 4.1

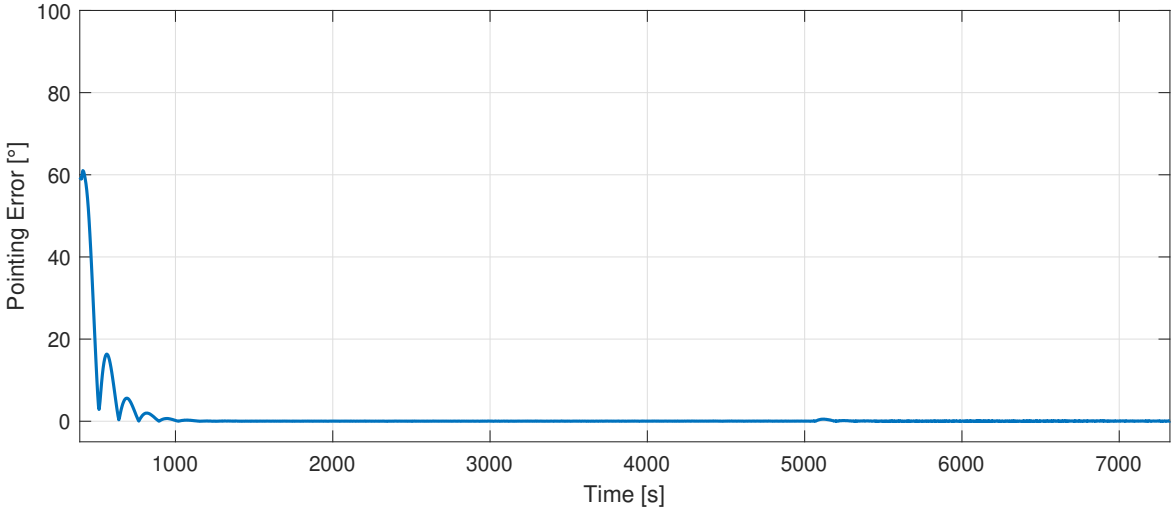

Figure 19: Pointing error off-design case 4.1

Considering :

$$\omega(0) = \begin{bmatrix} 0.3 & 0.3 & 0.3 \end{bmatrix}$$

the angular velocity, Fig. 20, control torque, Fig. 21, and pointing error, Fig. 22, can be evaluated.

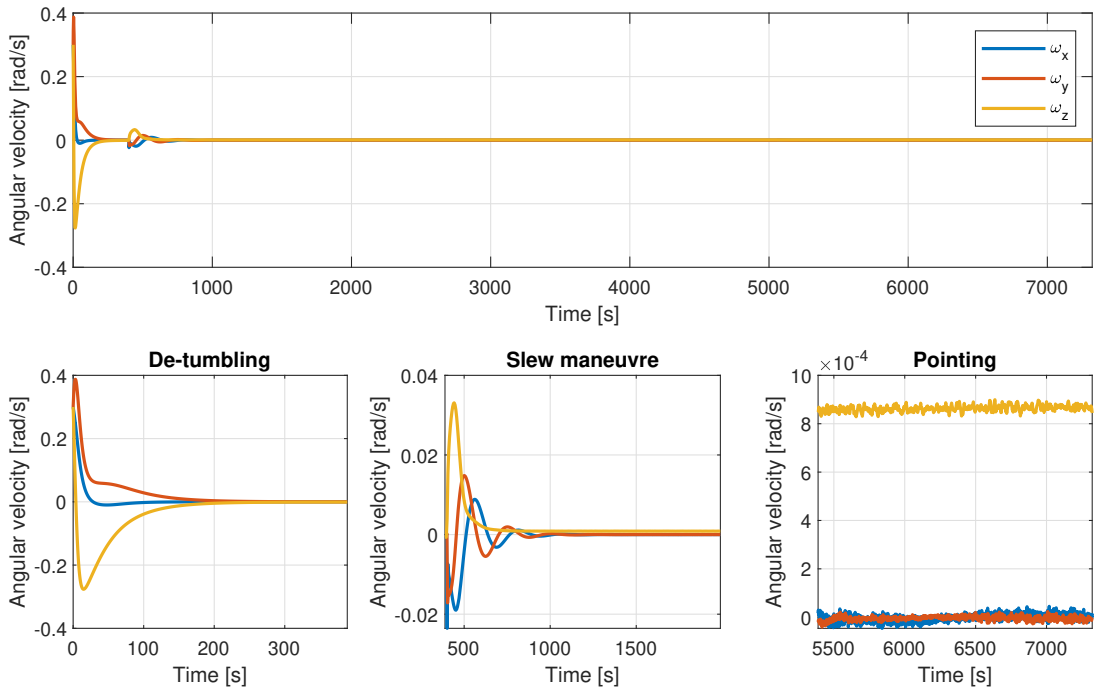

Figure 20: Angular velocities off-design case 4.2

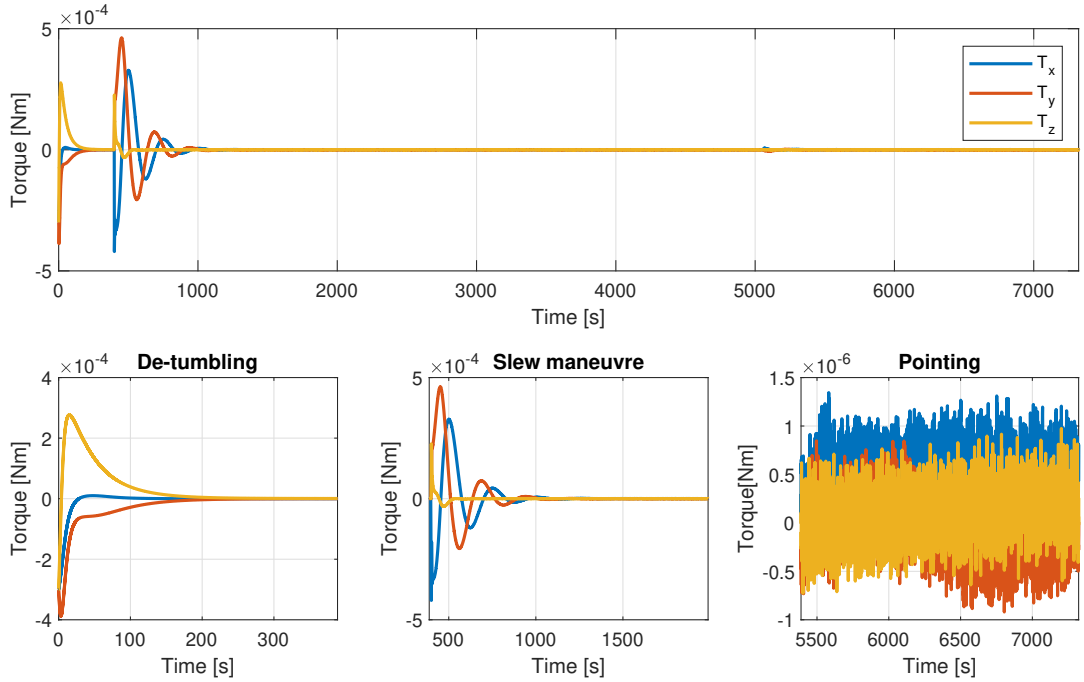

Figure 21: Control torque off-design case 4.2

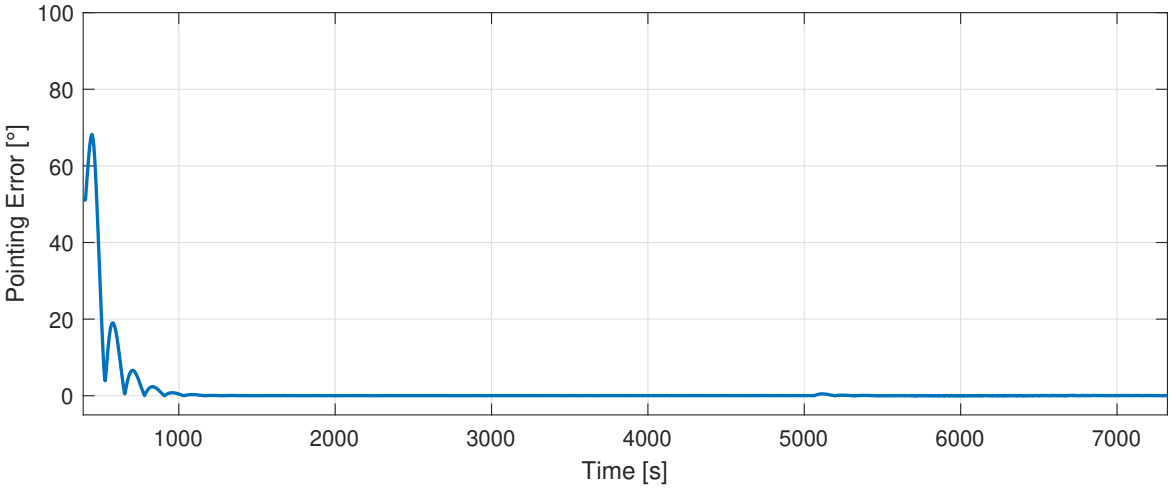

Figure 22: Pointing error off-design case 4.2

As expected, higher the initial angular velocity higher will be the torque that has to be provided. This has to be taken into account in order to avoid saturation of the reaction wheel. Simple solutions to avoid saturation are to limit the injection angular velocity, choose reaction wheels that can provide higher torque or add a redundant reaction wheel in order to distribute better the torque and avoid saturation using specific de-saturation technique.

8 Conclusions

The simulations performed have demonstrated that the ADCS here presented is capable to satisfy the detumbling and Earth pointing mission requirements, section 4, both in nominal and off-nominal conditions. The system can be improved adding a redundant reaction wheel in case of failure of one of the already used, or to have a de-saturation mechanism in case of highly demanding torque manoeuvres. The choice of a trial and error approach to determine the gains of the controller could be useful in case of a preliminary design. For better performances ad hoc techniques could be used to determine the gains or a different control logic could be implemented. The model implemented include all the main dynamics and perturbations of the real system, nevertheless it can be refined in order to achieve more realistic simulations. A complete model of the IGRF could be introduced, model of the main orbital perturbation could be taken into account, or a detailed analysis of the complete structure could be performed in order to have a more precise inertia matrix.

References

[1] *BCT Micro Reaction Wheel*. URL: http://mecaspa.cannes-aero-patrimoine.net/nanosatellite/documentation%20technique/BCT-micro-reaction-wheel-datasheet-1.11.pdf.

[2] *CubeSense N*. URL: https://www.satcatalog.com/component/cubesense-n/.

[3] Howard Curtis. *Orbital Mechanics for Engineering Students*. Elsevier LTD, Oxford, 2004.

[4] F.Bernelli. *Lecture notes for the course "Spacecraft Attitude Dynamics and Control"*.

[5] *FS100 Fine Sun Sensor*. URL: https://www.satcatalog.com/component/fss100-387/.

[6] Marcel J. Sidi. *Spacecraft Dynamics and Control - A Practical Engineering Approach*. Cambridge University Press, 1997.

[7] *NanoSense M315 GomSpace*. URL: https://gomspace.com/UserFiles/Subsystems/datasheet/gs-ds-nanosense-m315-12.pdf.

[8] *Sensonor STI210*. URL: https://www.sensonor.com/products/gyro-modules/stim210/.